Bulletin of Environmental Contamination and Toxicology
https://doi.org/10.1007/s00128-021-03358-6

Secondary Sulfate Minerals from Pyrite Oxidation in Lanmuchang Hg-Tl Deposit, Southwest Guizhou Province, China: Geochemistry and Environmental Significance

Fengqi Zhao[1] · Shangyi Gu[1,2] · Likai Hao[3] · Hongguang Cheng[3] · Lingfei Liu[3]

Received: 18 September 2020 / Accepted: 13 August 2021

Abstract
Thallium (Tl) is a highly toxic trace metal posing a significant threat to human health. Tl pollution in soils and chronic Tl poisoning related to Tl-rich sulfides weathering in the Lanmuchang mine of southwest Guizhou province, China, have been intensively studied in recent years. And yet, there are few studies on the role of secondary sulfate minerals associated with Tl mobility in this area. The sulfate minerals were characterized by XRD and SEM-EDS. The concentrations of Tl and other elements were determined by ICP-MS. The results show that sulfate minerals are predominantly melanterite, halotrichite, and fibroferrite. The average contents of Tl in rock, sulfate minerals, and soil samples were 156.4, 0.11, and 72.1 μg g^{-1}, respectively. This study suggests that Tl in the mineralized rocks entered soils by pyrite oxidation with less scavenged of the sulfate minerals. The dissolution of the ferric sulfate minerals accelerates pyrite oxidation and maintains soil acidity, and this likely enhances Tl mobility from soil to crops.

Keywords Thallium · Secondary sulfate minerals · Mobility · Lanmuchang · Pyrite oxidation

Acid mine drainage (AMD) is produced by a series of microbially-mediated redox reactions when the waste rocks or tailings generated during the mining and mineral processing of sulfide-bearing ores are exposed to the atmospheric oxygen and water. Due to its low pH values, high concentration of toxic elements, and sulfate contents, it often causes severe environmental contamination and ecological harm to the downstream (Nordstrom et al. 1982; Bigham and Nordstrom 2000; Wu et al. 2001; Romero et al. 2006). Secondary sulfate minerals can form from AMD when these minerals are saturated under suitable physical, chemical, and biological conditions. These secondary sulfate minerals may be intermediate sources of metals because of their high concentrations of trace metals (Hammarstrom et al. 2005). Most of these minerals are highly water-soluble, so their rapid dissolution usually exerts a dramatical impact on the metal load and downstream aquatic ecosystems (Nordstrom et al. 1982; Bigham and Nordstrom 2000; Frau 2000; Joeckel et al. 2005). As a result, the secondary sulfate minerals generally play a prominent role in metal sequestration and acid mine drainage produced by sulfide oxidation. Whereas some metals, such as Fe, Ni, Zn and Cu are readily scavenged by secondary sulfate minerals, others such as Sb and Tl may remain partly in solution, which represent a threat to living organisms (Hammarstrom et al. 2005; Coup et al. 2015).

Thallium is a trace element that exhibits both lithophile and chalcophile geochemical behavior, with an abundance of below 1 μg g^{-1} in the Earth's crust (Belzile and Chen 2017; George et al. 2019). Due to the similar ionic radii of Tl^+ and K^+, Tl is usually dispersed in alumino-phyllosilicates (e.g., K-feldspar and muscovite). Meanwhile, Tl is also enriched in sulfides under low temperature hydrothermal conditions (e.g., pyrite and lorandite). Thallium has both Tl^+ and Tl^{3+} oxidation states, and Tl^+ is the thermodynamically dominant species under most environmental conditions (Vink 1993; Casiot et al. 2011). Thallium is more toxic to living organisms than Cd, Pb, As,

✉ Shangyi Gu
sygu@gzu.edu.cn

1 College of Resource and Environmental Engineering, Guizhou University, Guiyang 550025, China

2 Key Laboratory of Karst Georesources and Environment, Guizhou University, Ministry of Education, Guiyang 550025, China

3 State Key Laboratory of Environmental Geochemistry, Chinese Academy of Sciences, Guiyang 550002, China

Published online: 21 August 2021

and Hg, and is listed by the U.S. Environmental Protection Agency as one of the priority pollutants for control (Aguilar-Carrillo et al. 2020).

In the 1960 and 1970s, about 200 cases of chronic Tl poisoning were reported in the southwest Guizhou province, China (Zhou 1981). It is commonly agreed that the mining process of the Lanmuchang Hg-Tl deposit in the area is closely related to the Tl poisoning (Xiao 2001; Lin et al. 2020). After the final closure of the mine during the 1980s, there are still large quantities of mining residues exposed to oxidative weathering, which poses a significant threat to the downstream ecosystems (Zhang et al. 1997; Xiao et al. 2004a, b; Lin et al. 2020). Previous studies have made much progress on the Tl sequestration mechanism in the contaminated soils, the enrichment of Tl in plants, and the impact on the microbial ecology. Reported concentrations of Hg and As in crops and vegetables were below Chinese national limit for contaminants (Xiao et al. 2004a, b). Despite the widespread distribution of pyrite-rich shales, little research on the mineralogy and environmental significance of secondary sulfate minerals in the mining area has been conducted so far. Considering the prevalence of secondary sulfate minerals in the Lanmuchang Hg-Tl mine, this study will focus on the geochemistry of these minerals and their role in the migration and mobilization of Tl.

Materials and Methods

The study area is located in Huilong town, Xingren county, southwest Guizhou province (Fig. 1). This area is a low hilly topography with elevations ranging from 1403 to 1510 m. The climate type is subtropical mild and moist monsoon with an average annual rainfall of 1250–1400 mm. The striking enrichment of Tl in Permian and Triassic argillite of this area is attributed to Tl mineralization (Chen 1989; Zhang et al. 2004). Thallium is typically occurring in various sulfide minerals, especially colloidal pyrite, which is one of the most important Tl-bearing minerals (Li 1996). Moreover, pyrite dominates the sulfides in both ores and mineralized rocks (Li 1996; Chen et al. 1998). Significant amounts of secondary sulfate minerals were observed in two adjoining abandoned adits during the field investigation (Fig. 2a, b). The soils in the Lanmuchang area are not well developed (oxisol), which are mainly derived from the weathering of surrounding mineralized rocks and mining spoil, and are intensively cultivated for crops.

Eight fresh and weathered rock, four secondary sulfate minerals, and ten cultivated topsoil (0–20 cm depth) samples were collected in the Lanmuchang area. The rock samples were cut into thin slices with a thickness of 0.03 mm for mineralogical examination under a polarizing microscope and ground to ≤75 μm in a planetary ball mill with agate-grinding for further analysis. The soil samples were air-dried

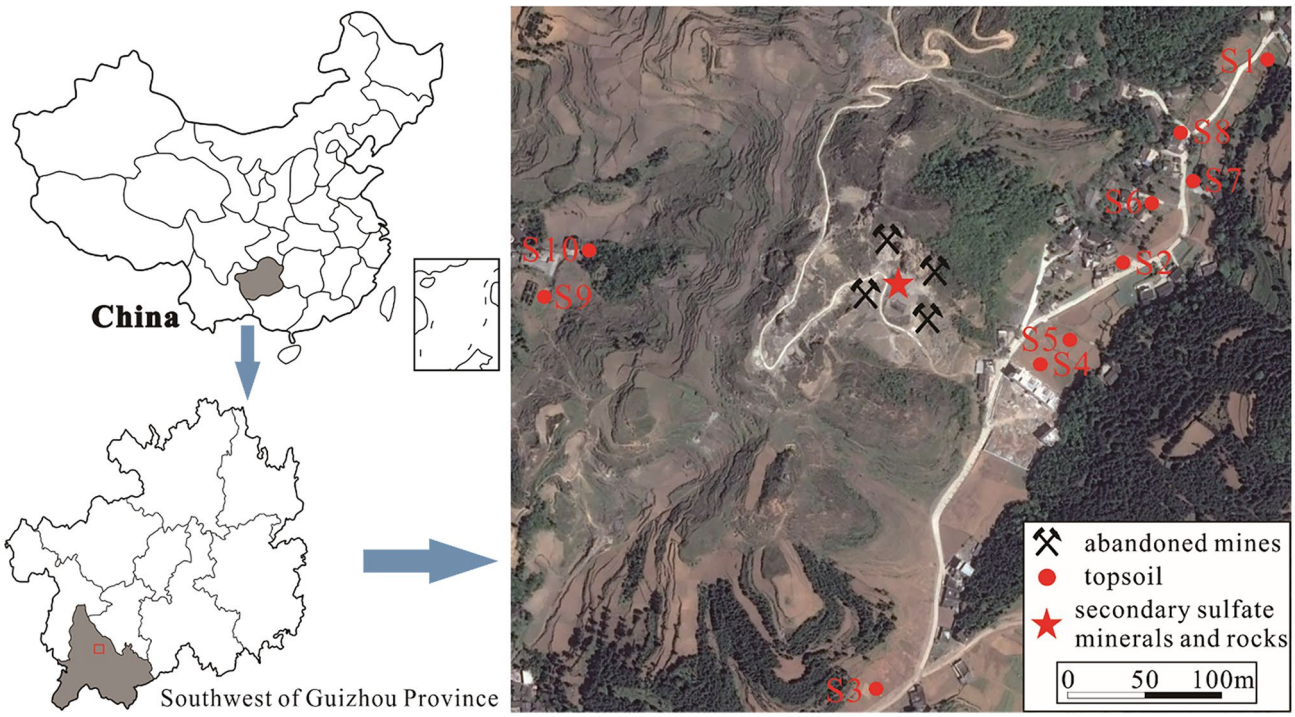

Fig. 1 Sketch maps showing the sampling locations in the Lanmuchang Hg-Tl deposit in Guizhou province

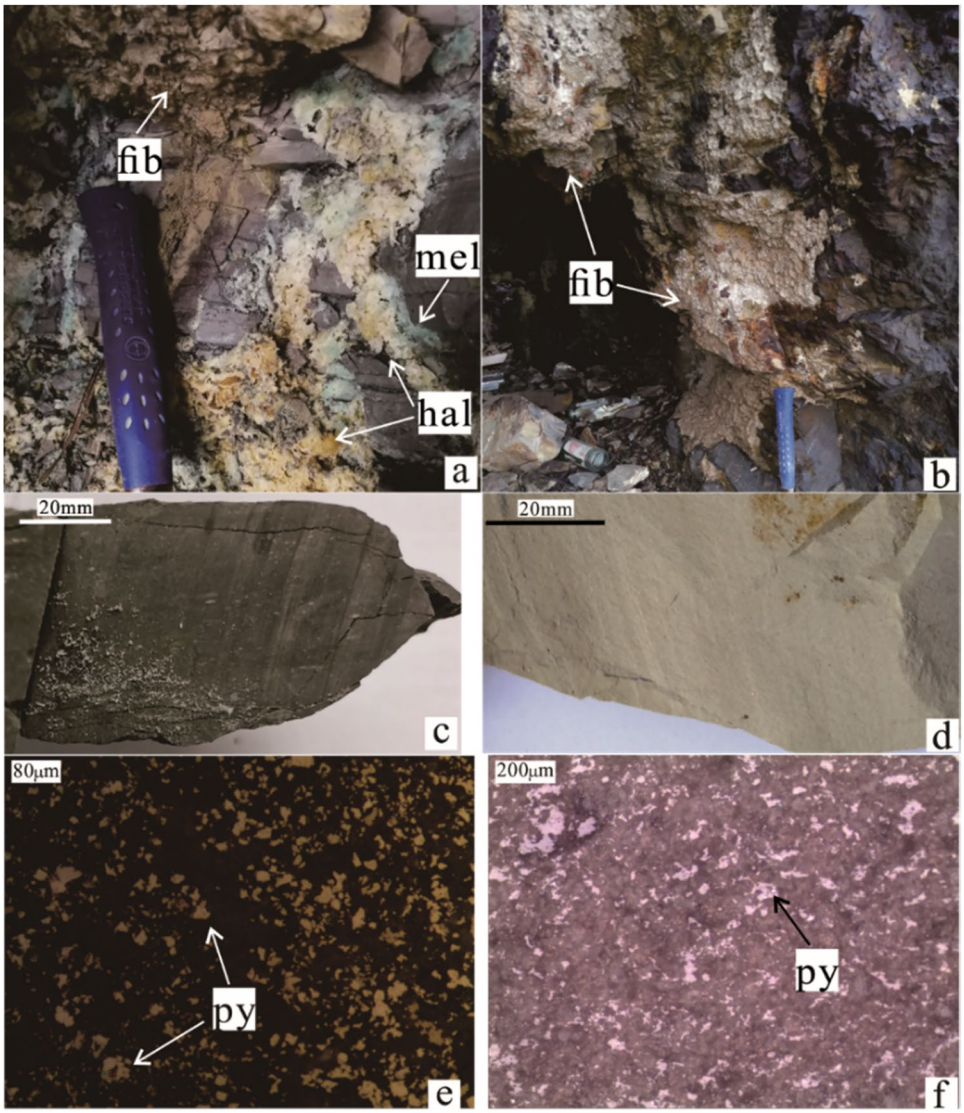

Fig. 2 The secondary sulfate minerals and pyrite in the host rocks from the Lanmuchang Hg-Tl abandoned mines in Guizhou province. **a** Melanterite (mel), halotrichite (hal) and fibroferrite (fib) in the surface of the host rock (hammer grip 20 cm). **b** Fibroferrite in the surface of the host rock (hammer grip 20 cm). **c** Fresh dark host rock. **d** Weathered host rock. **e** Microgranular pyrites (py) in the fresh rock under the polarizing microscope. **f** Trace pyrites in the weathered rocks under the polarizing microscope

at room temperature to constant weight. Then gently ground in a ceramic mortar and passed through an 18-mesh stainless steel sieve for pH measurement. Soil pH was measured using a calibrated pH meter (PHS-3 C, INESA) with a soil to deionized water ratio of 1:2.5 (weight/volume), whereas secondary sulfate minerals pH measurement was performed with a ratio of 1:10. The subsamples were continued ground to ≤ 75 μm prior to further analysis. The mineralogical composition of secondary sulfate and selected soil samples were characterized by X-ray diffraction (XRD). The powder XRD analyses were conducted on a model Empyrean X-ray diffractometer (Panalytical, Malvern, UK) with Cu *K*α radiation (40 kV and 40 mA). Samples were scanned from 2 to 70° 2θ with a 0.026° step and a 30-s count time. The XRD patterns were matched with the mineral diffraction files by a computer automatic search-match function but without using internal standards and only semi-quantitative estimations were made.

In order to observe the morphologies of secondary sulfate minerals and further verify the XRD identifications, the scanning electron microscopy with energy dispersive spectrometry (SEM-EDS) investigation were performed using an FEI Quanta FEG 250 field emission SEM-EDS (Thermo Fisher, Waltham, MA). Due to the thermal sensitivity of sulfate minerals, high vacuum and low acceleration voltage (6 kV) modes were selected to obtain high-quality images of the surface morphology of uncoated samples. EDS spectra were collected using a beam spot of 2.5 μm diameter at an accelerating voltage of 20 kV. Analytical standards of quartz (O), pyrite (S), corundum (Al) and iron (Fe) were chosen to semi-quantitatively estimate the main chemical composition of minerals.

The geochemical composition of selected rock, soil, and sulfate samples was determined by inductively coupled plasma–mass spectrometry (ICP-MS, iCAP RQ, Thermo Scientific, Waltham, MA) with detection limits in the

billionth. Before testing, the powdered soil/rock samples were digested with a PTFE bomb and PFA beaker by concentrated HNO_3-HF-HCl and the secondary sulfate samples were dissolved in ultrapure water to extract the supernatants by centrifugation. Quality assurance/quality control procedures were carried out by adding internal standards Rh and In to the sample solutions, combined with the reference materials (USGS W-2a) and the laboratory blanks, ensure that the relative errors of the trace elements were controlled within 2%.

Results and Discussion

Polarizing microscopic observation showed that the minerals in the mineralized rocks and waste rocks were mainly fine-grained quartz and clay minerals with different contents of pyrite (Fig. 2e, f). Pyrite occurs mainly as anhedral grains (average 20 μm diameter) distributed in the rocks (Fig. 2e). When the black shale weathered to gray (Fig. 2c, d), pyrite was almost completely disappeared from the slices (Fig. 2f). According to XRD analysis, the secondary sulfates minerals XR2 and XR4 are melanterite and fibroferrite, respectively, while XR1 and XR3 show a mixture of halotrichite and pickeringite in different proportions. Further analysis by EDS and ICP-MS revealed only minor amounts of Mg were present in XR1 and XR3 (Table 1; Fig. 3a). Thus, this pickeringite illusion is probably due to the similarity in d-spacing values, as noted by Jambor et al. (2000) in some cases no distinction is made between halotrichite and pickeringite. The XRD results indicated that the soil mineralogy is dominated by quartz, with small amounts of silicate minerals (Table 2). In addition, jarosite and barite also occurred in the selected soil samples.

Secondary sulfate minerals have a pH value of 4.49–4.88. The results showed that fibroferrite has the lowest pH value among the sulfate minerals, which is consistent with Frau's (2000) dissolution acid-producing experiments. The soil has a pH varying from 5.41 to 7.03. The Tl content in the rocks ranged from 10.2 to 427 μg g^{-1}, with an average value of 156.4 μg g^{-1}. Meanwhile, the Tl content decreased from 427 μg g^{-1} in slightly weathered rocks to 10.2 μg g^{-1} in intensively weathered. However, the Tl concentration in secondary sulfate minerals was only 0.052 to 0.149 μg g^{-1}. The Tl level in topsoil samples varied from 8.08 to 125 μg g^{-1}, with a mean value of 72.1 μg g^{-1}, which compares to the 1 μg g^{-1} maximum allowable environmental concentration (Aguilar-Carrillo et al. 2018), indicating that arable land in

Table. 1 Basic chemical characteristics of the rocks, sulfate minerals, and soils

Sample	Mg μg g^{-1}	Fe μg g^{-1}	Mn μg g^{-1}	Cr μg g^{-1}	Cu μg g^{-1}	Co μg g^{-1}	Ni μg g^{-1}	Tl μg g^{-1}	pH_{H2O}
LMC01	1280	73,500	5.89	55.7	65.4	25.7	57.8	131	
LMC02	1370	20,900	10.4	51.1	27.5	11.5	22.2	45.0	
LMC03	2630	3510	13.5	57.9	1.60	3.13	8.62	11.0	
LMC04	328	159,000	4.89	73.8	97.2	1.77	2.77	10.2	
LMC05	166	8260	4.07	24.7	12.3	2.91	33.3	427	
LMC06	417	127,000	10.9	50.3	108	29.2	56.5	382	
LMC07	454	26,800	5.71	46.9	20.2	6.64	17.0	167	
LMC08	195	2110	3.21	39.8	1.89	0.84	1.61	77.8	
XR1	109	69,800	5.47	101	85.0	146	60.9	0.149	4.53
XR2	149	331,000	3.90	3.97	703	156	147	0.052	4.88
XR3	86.9	69,200	3.87	97.5	168	135	52.6	0.100	4.57
XR4	119	154,000	13.6	27.0	74.0	139	49.4	0.141	4.49
S1	6940	86,900	733	97.0	147	41.9	82.3	16.1	5.76
S2	3190	68,400	511	105	102	17.7	42.9	120	5.87
S3	4320	102,000	1120	326	123	40.9	77.7	8.08	6.16
S4	5270	89,300	1070	106	119	34.6	69.2	124	5.41
S5	6300	82,100	610	100	131	32.5	69.7	23.5	5.76
S6	11,800	90,900	2080	113	135	51.3	82.9	49.5	5.86
S7	7130	82,700	1290	104	130	40.4	69.6	34.6	6.52
S8	5080	79,400	696	101	103	18.9	38.4	120	6.36
S9	3600	54,000	332	83.5	62.0	13.4	47.9	125	5.76
S10	4590	74,300	546	118	133	17.7	41.2	100	7.03

LMC01-LMC08, rock samples; XR1-XR4, sulfate mineral samples; S10, topsoil samples

Table. 2 Mineralogy (XRD-based) of the selected soil samples

Sample	Mineral												
	Qtz	Prl	Kln	Mnt	Ill	Am	Fsp	Cal	Dol	Hem	Ant	Brt	Jrs
S4	****	**	***	***	***	***	***	_	_	***	***	_	**
S5	****	**	***	***	**	**	**	*	**	**	***	_	*
S6	****	**	***	***	***	_	***	*	**	**	***	**	**
S8	****	**	***	***	**	**	**	_	_	***	***	***	***
S9	****	_	***	*	*	*	_	*	_	**	**	*	*
S10	****	_	***	**	*	**	_	*	*	**	***	_	***

Qtz quartz, *Prl* pyrophyllite, *Kln* kaolinite, *Mnt* montmorillonite, *Ill* illite, *Am* amphibole, *Fsp* feldspar, *Cal* calcite, *Dol* dolomite, *Hem* hematite, *Ant* anatase, *Brt* barite, *Jrs* jarosite

****Major component (> 80%)

***1–5%

**< 1%

*Presence

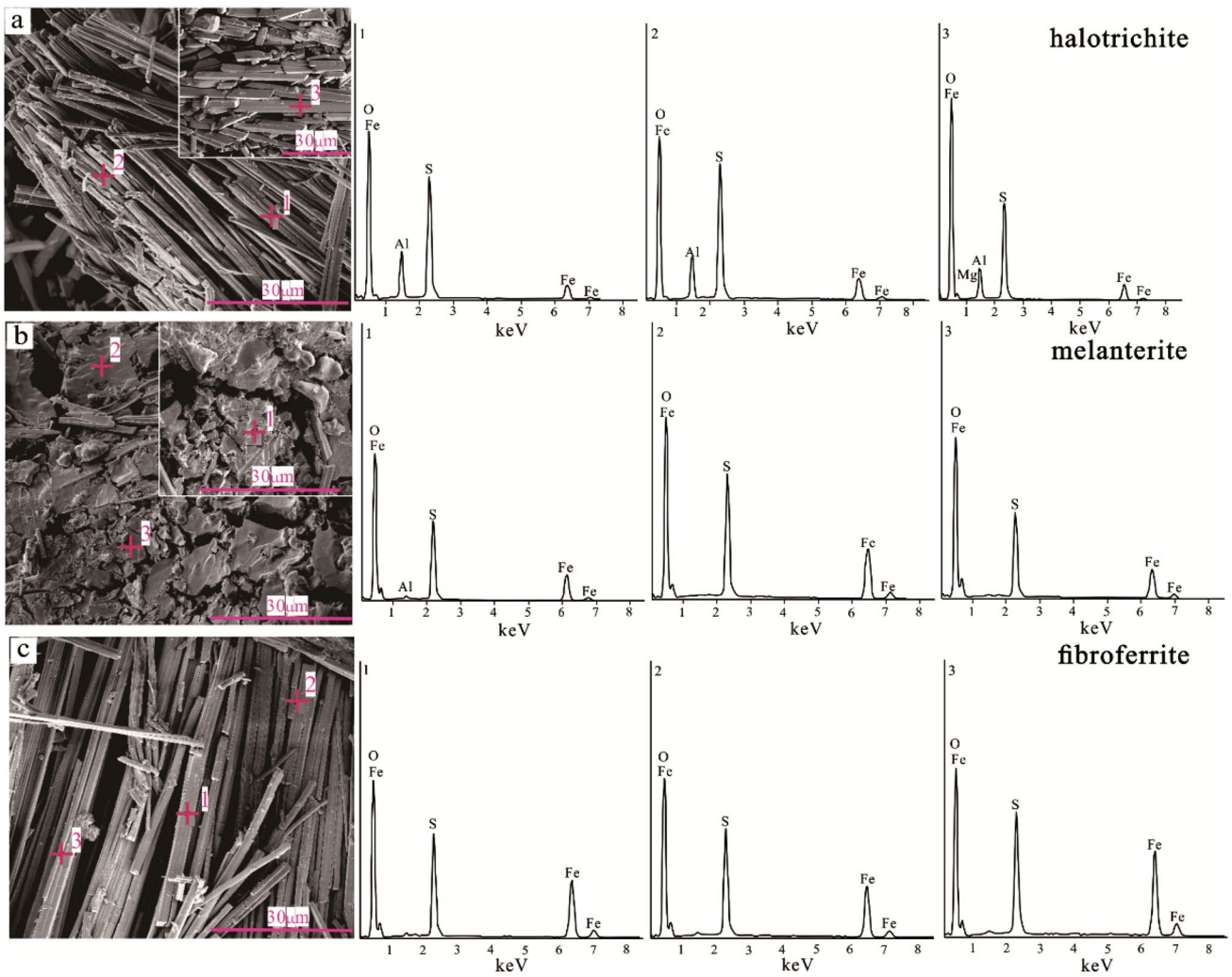

Fig. 3 Secondary sulfate minerals characterized by SEM-EDS from the Lanmuchang Hg-Tl deposit, Guizhou province. **a**, **b** and **c** correspond to SEM images of halotrichite, melanterite, and fibroferrite as well as EDS spectra of selected points, respectively

the area is severely contaminated. Expectedly, multiple crops and vegetables in the area are also seriously contaminated (Xiao 2001; Jia et al. 2013).

The rate of pyrite oxidation is closely related to the intensity of AMD, and crystal size is one of the critical factors in determining the rate of pyrite oxidation. In essence, those with smaller sizes usually have a higher oxidation rate because of their larger specific surface area (Frau 2000). The anhedral and fined grain sizes (about 20 μm) made the pyrite in the rocks susceptible to oxidation. A recent study indicates that Tl may be present in structural defects of pyrite (George et al. 2019), and this is also a site where pyrite is prone to oxidation (Frau 2000). From the aforementioned results, it can be seen that the vast majority of Tl is mobilized during the weathering of pyrite. As the elevated concentrations of metals were incorporated into the structure of secondary sulfate minerals, these minerals may be acting as temporary storage of metals (Nordstrom and Alpers 1999; Buckby et al. 2003). However, neither Lanmuchangite ($TlAlSO_4{\cdot}12H_2O$) nor jarosite [$KFe^{3+}3(SO_4)_2(OH)_6$], two Tl-rich sulfate minerals, were detected by XRD and SEM-EDS. We attribute these two sulfate minerals reported by Chen et al. (2003) from the Lanmuchang to the restricted condition and Tl ore oxidation.

Melanterite ($Fe^{2+}SO_4{\cdot}7H_2O$), fibroferrite [$Fe^{3+}(SO_4)(OH){\cdot}5H_2O$], and halotrichite [$Fe^{2+}Al_2(SO_4)_4{\cdot}22H_2O$] are prevailing secondary sulfate minerals from the surface samples of the mineralized rocks in the Lanmuchang. Thermodynamic data indicate that these sulfate minerals were formed in very acidic (pH < 3) environments through evaporation (Majzlan 2010). During rainfall or high humidity conditions, these minerals will release potential acidity and Fe^{2+}/Fe^{3+} ions through dissolution and deliquescence.

Ferric iron is a more important oxidant for pyrite than O_2 under acid conditions (Frau 2000; Jerz et al. 2003). Ferric iron can be provided indirectly through the dissolution and oxidation of Fe^{2+} minerals such as melanterite. It can also be supplied directly by Fe^{3+} minerals such as fibroferrite, thus forming a self-sustaining cycle (Singer and Stumm 1970) as the following reaction:

$$FeS_2+7/2O_2+H_2O \rightarrow Fe^{2+}+2SO_4^{2-}+2H^+ \quad (1)$$

$$Fe^{2+}+1/4O_2+H^+ \rightarrow Fe^{3+}+1/2H_2O \quad (2)$$

$$Fe^{3+}+3H_2O \rightarrow Fe(OH)_3+3H^+ \quad (3)$$

$$FeS_2+14Fe^{3+}+8H_2O \rightarrow 15Fe^{2+}+2SO_4^{2-}+16H^+ \quad (4)$$

The oxidation of ferrous iron to ferric iron is a rate-limiting step at the low pH (~3), which needs microbial catalysis to overcome the extremely slow rate in abiotic conditions (Singer and Stumm 1970). The hydrolysis of ferric iron to $Fe(OH)_3$ (reaction (3)) could cover the surface of the pyrite or further oxidize the pyrite (reaction (4)) depends on the pH value of the solutions. In acidic pH conditions as indicated by the secondary sulfate minerals, the ferric iron may remain in the dissolved state and sustain the above-mentioned self-sustaining cycle (Hammarstrom et al. 2005). Actually, the pH of rock surfaces will maintain a much lower level in the presence of large amounts of secondary sulfate minerals, as demonstrated by Frau (2000). Tl in secondary sulfate minerals is 2–3 orders of magnitude lower than in rocks, we reveal that the secondary sulfate minerals are not temporary storage for Tl in the Lanmuchang. Alternatively, these secondary sulfate minerals produced on and covering the rock surfaces likely accelerate the oxidation and Tl release process of pyrite in the rocks. This hypothesis is also supported by the more severe weathering of rocks covered with fibroferrite observed in the field. The concentrations of Cr, Cu, Co, and Ni were generally 2–3 orders of magnitude higher than Tl, indicating that these secondary metal sulfate minerals may be a transient sink for these metals. Melanterite contains up to 703 μg g^{-1} of Cu, suggesting a high sequestration capacity of Cu in melanterite formed under natural conditions as found in previous studies (Hammarstrom et al. 2003; Romero et al. 2006) and laboratory experiments (Basallote et al. 2019). Since Tl^+ is the most stable species and exists predominantly as free ions in aqueous solution (Kaplan and Mattigod 1998; Xiong 2009; Perotti et al. 2017), the mobilized Tl will spread rapidly downstream with rain and streamflow.

The range of Tl concentrations and pH values in the soil is consistent with previous reports in the area (Xiao et al. 2004a, b; Jia et al. 2018; Lin et al. 2020). It is noteworthy that jarosite is occured in topsoil samples, especially those with high Tl content. The presence of jarosite indicates that the soil is still affected by AMD. Jarosite has an excellent ability to retain Tl during its formation (Dutrizac 1997; Aguilar-Carrillo et al. 2020). Elevated Tl content in jarosite has been reported in the Lanmuchang area (Xiao 2001; Zhang et al. 2004; Lin et al. 2020). Similar to the sulfate minerals mentioned above, jarosite is formed in a very acidic environment. It is reported that Tl can form dorallcharite [$Tl_{0.8}K_{0.2}Fe_3(SO_4)_2(OH)_6$] in supergenic conditions (Ballczunlc et al. 1994), implying that substitution by Tl for potassium in the jarosite-alunite family. At 3.5 < pH < 7.5, the dissolution of jarosite will release the sequestered Tl and results in the formation of more stable hematite and ferrihydrite, which is also an acid-producing process (Elwood Madden et al. 2012). The measured soil pH values are within the range mentioned above. Therefore, jarosite in the soils of Lanmuchang is a transient sink source for Tl. However, hematite formed by the dissolution of jarosite is also an important secondary Tl-bearing mineral phase in this

region (Lin et al. 2020), which will lead to more persistent contamination.

It has been previously reported that most Tl in the soils of Lanmuchang is within the residual fractions in operationally defined speciation procedures (Jia et al. 2013, 2018), which is generally closely associated with aluminosilicate minerals such as illite (Gomez-Gonzalez et al. 2015). Both experimental studies (Martin et al. 2018; Wick et al. 2018) and field investigation (Voegelin et al. 2015) have confirmed that illite is one of the most important adsorbents of Tl. Based on the fact that Tl adsorption onto the aluminosilicate minerals is pH-dependent (Martin et al. 2018), which is expected to favor the desorption of Tl under acidic soil conditions and its uptake by crops.

In summary, we found that the secondary sulfate minerals in the mineralized rocks from the Lanmuchang mine enhanced pyrite oxidation and Tl release from the rocks. The jarosite in the soils is a transient source of Tl at Lanmuchang. Mineralogical transformation of jarosite in acidic soils will result in longer-lasting contamination and suggest that the solid-phase control of Tl is dynamically changing. The acidic soil environment generated by pyrite oxidation and maintained by jarosite dissolution can, to some extent, promote the uptake of Tl by crops and exert health impacts to the local residents.

Acknowledgements This work was funded by the National Key R&D Program of China (No. 2018YFC1802601) and the Science and Technology Planning Project of Guizhou province [(2018)1177].

References

Aguilar-Carrillo J, Herrera L, Gutiérrez EJ, Reyes-Domínguez IA (2018) Solid-phase distribution and mobility of thallium in mining-metallurgical residues: environmental hazard implications. Environ Pollut 243:1833–1845

Aguilar-Carrillo J, Herrera-García L, Reyes-Domínguez IA, Gutiérrez EJ (2020) Thallium(I) sequestration by jarosite and birnessite: structural incorporation vs surface adsorption. Environ Pollut 257:1–11

Ballčžunlc T, Moelo Y, Loncar Ž, Micheelsen H (1994) Dorallcharite $Tl_{0.8}K_{0.2}Fe_3(SO_4)_2(OH)_6$, a new member of the jarosite-alunite family. Eur J Miner 6(2):255–264

Basallote MD, Cánovas CR, Olías M, Pérez-López R, Macías F, Carrero S, Ayora C, Nieto JM (2019) Mineralogically-induced metal partitioning during the evaporative precipitation of efflorescent sulfate salts from acid mine drainage. Chem Geol 530:1–11

Belzile N, Chen YW (2017) Thallium in the environment: a critical review focused on natural waters, soils, sediments and airborne particles. Appl Geochem 84:218–243

Bigham JM, Nordstrom DK (2001) Iron and aluminum hydroxysulfates from acid sulfate waters. Rev Miner Geochem 40(1):351–403

Buckby T, Black S, Coleman ML, Hodson ME (2003) Fe-sulphate-rich evaporative mineral precipitates from the RíoTinto, southwest Spain. Miner Mag 67(2):263–278

Casiot C, Egal M, Bruneel O, Verma N, Parmentier M, Elbaz-Poulichet F (2011) Predominance of Aqueous Tl(I) Species in the River System Downstream from the Abandoned Carnoulès Mine (Southern France). Environ Sci Technol 45:2056–2064

Chen DY (1989) The discovery of lorandite in China and its study. Acta Miner Sin 9(2):141–147 (**in Chinese with English abstract**)

Chen DY, Ren DY, Wang H, Zou ZX, Qin Y (1998) Where is the second thallium ore deposit of Lanmuchang type?—The discovery of Yangjiawan thallium deposit prospect and its prospecting potentiality. J Guizhou Univ Tech 27(5):18–26 (**in Chinese with English abstract**)

Chen DY, Wang GX, Zou ZX, Chen YM (2003) Lanmuchangite, a new thallium (Hydrous) sulphate from Lanmuchang, Guizhou Province, China. Chin J Geochem 22(2):185–192

Coup KM, Swedlund PJ (2015) Demystifying the interfacial aquatic geochemistry of thallium(I): new and old data reveal just a regular cation. Chem Geol 398:97–103

Dutrizac JE (1997) The behavior of thallium during jarosite precipitation. Metall Mater Trans B 28B:765–775

Elwood Madden ME, Madden AS, Rimstidt JD, Zahrai S, Kendall MR, Miller MA (2012) Jarosite dissolution rates and nanoscale mineralogy. Geochim Cosmochim Acta 91:306–321

Frau F (2000) The formation-dissolution-precipitation cycle of melanterite at the abandoned pyrite mine of Genna Luas in Sardinia, Italy: environmental implications. Miner Mag 64(6):995–1006

George LL, Biagioni C, Lepore GO, Lacalamita M, Agrosì G, Capitani GC, Bonaccorsi E, d'Acapito F (2019) The speciation of thallium in (Tl, Sb, As)-rich pyrite. Ore Geol Rev 107:364–380

Gomez-Gonzalez MA, Garcia-Guinea J, Laborda F, Garrido F (2015) Thallium occurrence and partitioning in soils and sediments affected by mining activities in Madrid province (Spain): soil–plant transfer and influencing factors. Sci Total Environ 536:268–278

Hammarstrom JM, Seal II, Meier RR, Jackson ALJC (2003) Weathering of sulfidic shale and copper mine waste: secondary minerals and metal cycling in Great Smoky Mountains National Park, Tennessee, and North Carolina, USA. Environ Geol 45:35–350

Hammarstrom JM, Seal IIRR, Meier AL, Kornfeld JM (2005) Secondary sulfate minerals associated with acid drainage in the eastern US: recycling of metals and acidity in surficial environments. Chem Geol 215:407–431

Jambor JL, Nordstrom DK, Alpers CN (2000) Metal-sulfate salts from sulfide mineral oxidation. Rev Miner Geochem 40(1):303–350

Jerz JK, Rimstidt JD (2003) Efflorescent iron sulfate minerals: paragenesis, relative stability, and environmental impact. Am Miner 88:1919–1932

Jia YL, Xiao TF, Zhou GZ, Ning ZP (2013) Thallium at the interface of soil and green cabbage (*Brassica oleracea* L. *var. capitata* L.): soil–plant transfer and influencing factors. Sci Total Environ 450–451:140–147

Jia YL, Xiao TF, Sun JL, Yang F, Baveye P (2018) Microcolumn-based speciation analysis of thallium in soil and green cabbage. Sci Total Environ 630:146–153

Joeckel RM, Ang Clement BJ, VanFleet Bates LR (2005) Sulfate-mineral crusts from pyrite weathering and acid rock drainage in the Dakota Formation and Graneros Shale, Jefferson County, Nebraska. Chem Geol 215:433–452

Kaplan D, Mattigod S (1998) Aqueous geochemistry of thallium. Wiley, New York, pp 15–29

Li GZ (1996) A study of compositions and thallium occurrence in mercury-thallium deposits at Lanmuchang of Xinren County in Southwestern Guizhou. Guizhou Geol 13(1):24–37 (**in Chinese with English abstract**)

Lin JF, Yin ML, Wang J, Liu J, Tsang DCW, Wang YX, Lin M, Li HC, Zhou YY, Song G, Chen YH (2020) Geochemical fractionation

of thallium in contaminated soils near a large-scale Hg-Tl mineralised area. Chemosphere 239:1–8

Majzlan J (2010) Advances and gaps in the knowledge of thermodynamics and crystallography of acid mine drainage sulfate minerals. Chimia 64(10):699–704

Martin LA, Wissocq A, Benedetti MF, Latrille C (2018) Thallium (Tl) sorption onto illite and smectite: implications for Tl mobility in the environment. Geochim Cosmochim Acta 230:1–16

Nordstrom DK (1982) Aqueous pyrite oxidation and the consequent formation of secondary minerals. Wiley, New York, pp 37–56

Nordstrom DK, Alpers CN (1999) Negative pH efflorescent mineralogy and consequences for environmental restoration at the Iron Mountain Superfund site California. Proc Natl Acad Sci USA 96(7):3455–3462

Perotti M, Petrini R, D'Orazio M, Ghezzi L, Giannecchini R, Vezzoni S (2017) Thallium and Other Potentially Toxic Elements in the Baccatoio Stream Catchment (Northern Tuscany, Italy) Receiving Drainages from Abandoned Mines. Mine Water Environ 37:431–441

Romero A, González I, Galán E (2006) The role of efflorescent sulfates in the storage of trace elements in stream waters polluted by acid mine-drainage: the case of Peña Del Hierro, Southwestern Spain. Can Miner 44:1431–1446

Singer PC, Stumm W (1970) Acidic mine drainage: the rate-determining step. Science 167(3921):1121–1123

Vink BW (1993) The behaviour of thallium in the (sub) surface environment in terms of Eh and pH. Chem Geol 109:119–123

Voegelin A, Pfenninger N, Petrikis J, Majzlan J, Plötze M, Senn AC, Mangold S, Steininger R, Göttlicher J (2015) Thallium Speciation and Extractability in a Thallium- and Arsenic-Rich Soil Developed from Mineralized Carbonate Rock. Environ Sci Technol 52:5390–5398

Wick S, Baeyens B, Fernandes MM, Voegelin A (2018) Thallium Adsorption onto Illite. Environ Sci Technol 52:571–580

Wu P, Liu CQ, Yang YG, Zhang GP (2001) Release and transport of (heavy) metals and their environmental effect in mining activities. Acta Miner Sin 21(2):214–218 (**in Chinese with English abstract**)

Xiao TF (2001) Environmental impact of thallium related to the mercury-thallium-gold mineralization in Southeast Guizhou Province, China. Dissertation, University of Quebec

Xiao TF, He LB, Chen JA (2004) Aqueous environmental geochemistry of thallium in a thallium contaminated area of Southwest Guizhou. Earth Environ 32(1):35–41 (**in Chinese with English abstract**)

Xiao TF, Guha J, Boyle D (2004b) High thallium content in rocks associated with Au–As–Hg–Tl and coal mineralization and its adverse environmental potential in SW Guizhou, China. Geochem Explor Environ Anal 4:243–252

Xiong Y (2009) The aqueous geochemistry of thallium: speciation and solubility of thallium in low temperature systems. Environ Chem 6:441–451

Zhang BG, Zhang Z, Zhang XM, Chen GL (1997) A research into environmental geochemistry of Lanmuchang thallium deposit in Xinren of Guizhou Province. Guizhou Geol 14(1):71–77 (**in Chinese with English abstract**)

Zhang BG, Zhang Z, Hu J, Tian YF (2004) Thallium geochemistry and its ultra-normal enrichment. Guizhou Geol 21(4):240–244 (**in Chinese with English abstract**)

Zhou DX, Li SS (1981) Preliminary investigation on control and preventation of soil pollution by thallium. Acta Pedol Sin 19(4):409–411 (**in Chinese with English abstract**)